Transverse Spin Selectivity in Helical Nanofibers Prepared without Any Chiral Molecule

Chenchen Wang,[1,2,*] Zeng-Ren Liang,[3,*] Xiao-Feng Chen,[3] Ai-Min Guo,[3,†] Guanghao Ji,[1,2] Qing-Feng Sun,[4,5] and Yong Yan[1,2,6,‡]

[1]*CAS Key Laboratory of Nanosystem and Hierarchical Fabrication, CAS Center for Excellence in Nanoscience, National Center for Nanoscience and Technology, Beijing 100190, China*

[2]*University of Chinese Academy of Sciences, Beijing 100049, China*

[3]*Hunan Key Laboratory for Super-microstructure and Ultrafast Process, School of Physics, Central South University, Changsha 410083, China*

[4]*International Center for Quantum Materials, School of Physics, Peking University, Beijing 100871, China*

[5]*Hefei National Laboratory, Hefei 230088, China*

[6]*Department of Chemistry, School of Chemistry and Biological Engineering, University of Science and Technology Beijing, Beijing 100083, China*

(Received 17 October 2023; revised 14 May 2024; accepted 29 July 2024; published 4 September 2024)

In the last decade, chirality-induced spin selectivity (CISS) has undergone intensive study. However, there remain several critical issues, such as the microscopic mechanism of CISS, especially transverse CISS where electrons are injected perpendicular to the helix axis of chiral molecules, quantitative agreement between experiments and theory, and at which level the molecular handedness is key to the CISS. Here, we address these issues by performing a combined experimental and theoretical study on conducting polyaniline helical nanofibers which are synthesized in the absence of any chiral species. Large spin polarization is measured in both left- and right-handed nanofibers for electrons injected perpendicular to their helix axis, and it will be reversed by switching the nanofiber handedness. We first develop a theoretical model to study this transverse CISS and quantitatively explain the experiment. Our results reveal that our theory provides a unifying scheme to interpret a number of CISS experiments, quantitative agreement between experiments and numerical calculations can be achieved by weak spin-orbit coupling, and the supramolecular handedness is sufficient for spin selectivity without any chiral species.

DOI: 10.1103/PhysRevLett.133.108001

Introduction—Since the original experiment of asymmetric scattering of spin-polarized photoelectrons by chiral molecules [1], chirality-induced spin selectivity (CISS) has undergone intensive study [2–4] and showed great promise in spintronics [5–9], enantioseparation [10–15], and biological processes [16–18]. This CISS refers to longitudinal CISS, where spin selectivity occurs for electrons injected parallel to the helix axis. The longitudinal CISS was demonstrated in various chiral materials, including double-stranded DNA [19–24], single-helical protein or peptide [25–30], supramolecular polymers [31–35], and other organic compounds [36–50], most of which are composed of chiral building blocks, and the issue at which level the molecular handedness is key to the CISS arises naturally [36]. Many theories were proposed to elucidate this longitudinal CISS and the microscopic mechanism remains elusive [51–71].

Very recently, Naaman *et al.* measured the spin transport through supramolecular polymers containing achiral monomers, finding that they present spin filtering for electrons injected perpendicular to the polymer helix axis [72]. This is called transverse CISS and confirmed in another supramolecular structure [73]. In most previous experiments, however, chiral precursors were involved in preparing chiral materials [19–31,33–50], and subsequently they may reside on chiral materials synthesized and contribute to spin-selective measurements [72]. In particular, all previous theoretical studies focused on the longitudinal CISS [51–70], and the transverse CISS has not yet been addressed. And a large gap remains between experiments and theory [74–76], showing that quantitative agreement between experiments and numerical calculations seems impossible by using single-electron models [77].

In this Letter, we study the transverse CISS in helical nanofibers prepared from achiral polyanilines (PANIs) without any chiral precursor. By performing magnetic-conductive atomic force microscopy (mc-AFM), the spin-dependent electron transport is measured by injecting electrons normal to the nanofiber helix axis [Fig. 1(a)], finding that the spin polarization achieves ∼70% and is reversed by switching the nanofiber handedness. We first propose a theoretical model with extremely weak spin-orbit

*These authors contributed equally to this work.

†Contact author: aimin.guo@csu.edu.cn

‡Contact author: yany@nanoctr.cn

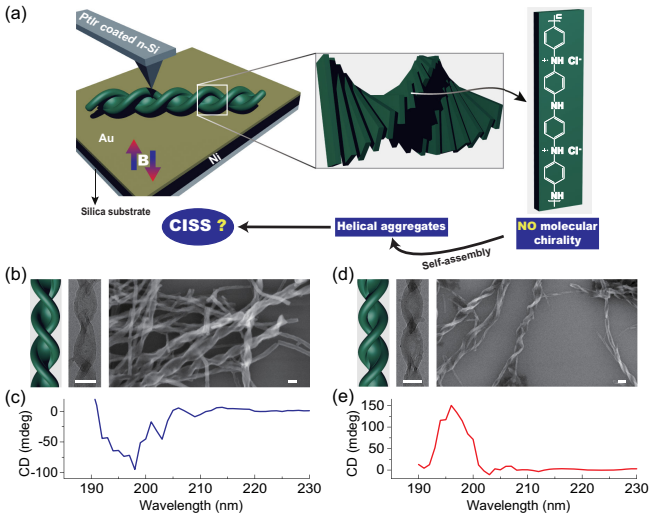

FIG. 1. Experimental setup, materials, and CD spectra. (a) Schematics of mc-AFM measurements on PANI left-handed nanofiber (left) and molecular structure of HCl doped PANI (right). Schemes (left), TEM (middle, scale bars, 50 nm), and SEM (right, scale bars, 100 nm) images of (b) left- and (d) right-handed nanofibers. (c) and (e) CD spectra of both nanofibers.

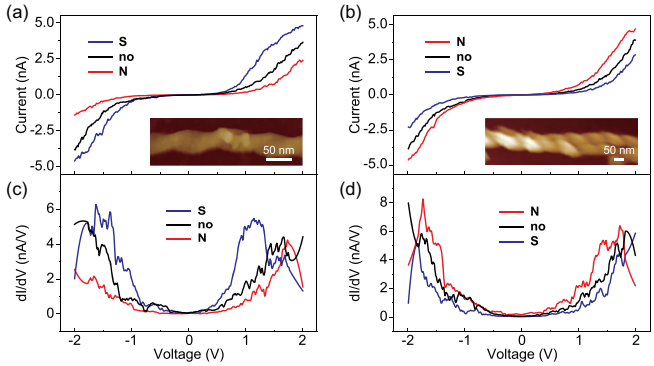

FIG. 2. Transverse CISS of PANI helical nanofibers. Current-voltage characteristics of (a) left- and (b) right-handed nanofibers when the lower Au/Ni electrode is magnetized downward (blue curves) or upward (red curves) by a magnet. The measurement is also conducted in the absence of magnetization (black curves). The insets in (a) and (b) are the AFM images of these nanofibers with scale bars being 50 nm. All the I-V curves are averaged over 50 measurements. Corresponding $dI/dV \sim V$ for (c) left- and (d) right-handed nanofibers.

coupling (SOC) to study this transverse CISS and quantitatively interpret the experiment, revealing that quantitative agreement between experiments and theory is possible by considering the single-electron picture.

Experiment—The PANI helical nanofibers are synthesized according to previous method [78,79], where aniline monomers are oxidized by ammonium persulfate in the mixed solvent of water and isopropyl alcohol [80]. A small amount of hydrochloric acid is added as the dopant. In the whole polymerization process, there are no chiral reagents and solvents. Besides, the reaction container is highly symmetric (cylinder glass vial), which will not impose any structural influence on polymer growth. Moreover, the polymerization is proceeded in a homogeneous solution without agitation, and thus the interfacial effect and vortex flow commonly used to assemble achiral materials and molecules into chiral aggregates are not applicable.

Interestingly, enantiomeric excess of PANI helical nanofibers is produced by adjusting the ratio of isopropyl alcohol to water in the solvent. For example, almost pure left-handed nanofibers are obtained when the solvent contains 35% isopropyl alcohol (v/v) [Figs. 1(b) and 1(c)]. By increasing alcohol content to 45%, the polarity environment changes and subsequently the nanofiber handedness becomes inverse [Figs. 1(d) and 1(e)]. The symmetry breaking and chirality inversion may originate from the cooperative effect of hydrogen bonding and π-stacking between neighboring PANIs [78,79].

Then, the spin transport through these nanofibers is measured by means of mc-AFM when the electrons are injected normal to their helix axis. The lower electrode is ferromagnetic and composed of a 150-nm-thick Ni layer covered with 10-nm-thick Au overlayer [Fig. 1(a)] [80]. With magnetic field, the electrons in the Ni layer become spin polarized and are injected into the PANI nanofibers. The current-voltage characteristics of left- and right-handed nanofibers are shown in Figs. 2(a) and 2(b), respectively. For the left-handed nanofiber, the current is larger when the lower Au/Ni electrode is magnetized downward by a magnet (0.35 T for at least 30 mins), as can be seen from the blue curve of Fig. 2(a). When the lower electrode is magnetized upward by reversing the magnetic field, the current is decreased [see the red curve of Fig. 2(a)]. Before magnetization of the Ni electrode, the current is measured for reference [see the black curve of Fig. 2(a)].

Remarkably, these observations in the left-handed nanofiber are reversed in the right-handed one, where the upward (downward) magnetization refers to larger (smaller) current [Fig. 2(b)]. This apparent spin-selective transmission is confirmed by plotting $dI/dV \sim V$, which qualitatively describes the effective "barrier" of electron hopping within these π-conjugated systems. For the left-handed nanofiber, the lowest barrier is found when the lower electrode is magnetized downward [see the blue curve of Fig. 2(c)]. However, this downward magnetization corresponds to the highest barrier in the right-handed nanofiber [see the blue curve of Fig. 2(d)]. In both nanofibers, the barrier heights of nonmagnetized devices lie between two magnetization cases [see the black curves of Figs. 2(c) and 2(d)].

The spin-selective capability of these nanofibers is then evaluated by calculating the current ratio $SP = (I_S - I_N)/(I_S + I_N)$ [86], where I_S and I_N are the measured currents when the lower Ni electrode is magnetized downward and upward, respectively. Positive and negative

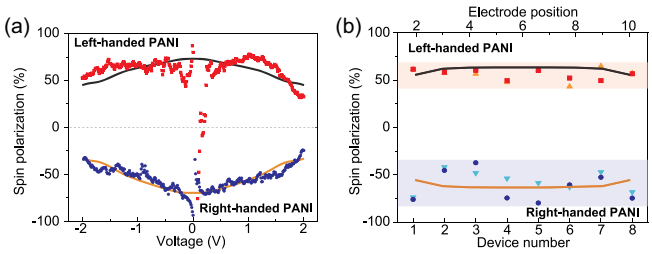

FIG. 3. Spin selectivity of PANI helical nanofibers. (a) Experimental (symbols) and theoretical (lines) results of voltage-dependent *SP* for left- and right-handed nanofibers. (b) Experimental (symbols, bottom x axis) and theoretical (lines, top x axis) *SP* for different nanofibers and/or different positions of the same nanofiber coupled to the upper electrode. Here, the red squares, orange-up triangles, and black lines correspond to left-handed nanofibers, and the remaining symbols and orange lines to right-handed nanofibers.

SP is obtained for left- and right-handed nanofibers [see the red squares and blue circles of Fig. 3(a)], respectively. The *SP* for both nanofibers achieves approximately 70%, which is comparable to the value for longitudinal CISS observed in other devices fabricated by chiral building blocks [31,33,34]. Besides, the *SP* gradually declines with increasing the voltage.

To confirm the reliability of our results, all the current-voltage curves are averaged over 50 individual measurements [80]. This is repeated an additional seven times by randomly selecting different helical nanofibers and/or different positions of the same nanofiber, namely, eight independent measurements for both left- and right-handed nanofibers. Similar current-voltage curves are observed for different nanofiber devices [80], and the *SP* of all these devices is summarized as the symbols in Fig. 3(b). We can see that all the left- and right-handed nanofibers display, respectively, positive and negative *SP* values with relatively small deviations. Furthermore, the *SP* remains essentially unchanged when the Au overlayer is decreased to 5 nm and is declined when it becomes thicker [80].

Model—A theoretical model is developed to unveil the transverse CISS in helical nanofibers, the schematic of which is shown in Fig. 4(a). As there are no magnetic atoms in PANIs, the SOC will be the key factor for the CISS [51–53]. Specifically, we assume that the SOC exists only in chiral coupling between neighboring PANIs but it vanishes inside an achiral PANI. In Fig. 4(a), each straight line parallel to the x-y plane denotes an achiral PANI, and all the lines self-assemble into a chiral nanofiber whose helix axis points along the z axis. We consider a nanofiber device contacted by a single upper nonmagnetic electrode and several lower magnetic electrodes, and its electron transport can be described by the Hamiltonian

$$\mathcal{H} = \mathcal{H}_{\mathrm{P}} + \mathcal{H}_{\mathrm{SOC}} + \mathcal{H}_{\mathrm{U}} + \mathcal{H}_{\mathrm{L}} + \mathcal{H}_{\mathrm{d}}. \tag{1}$$

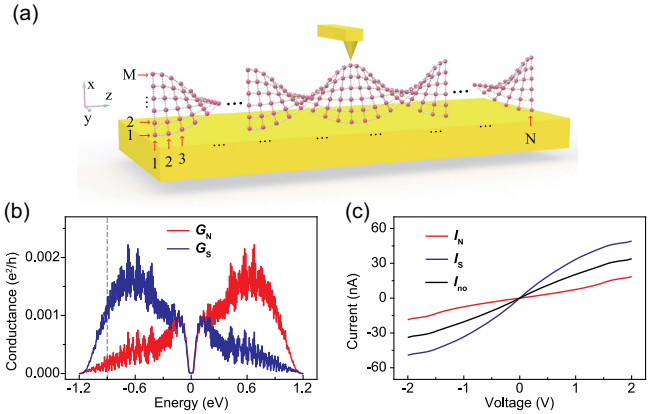

FIG. 4. Schematic of the theoretical model of the left-handed nanofiber and its numerical results. (a) Schematic of the left-handed nanofiber contacted by a single upper nonmagnetic electrode and several lower magnetic electrodes, where each ball denotes an aniline and self-assembles into an achiral PANI (straight line parallel to the x-y plane). (b) Energy-dependent conductance G_{N} with upward magnetization and G_{S} with downward magnetization. (c) Current-voltage characteristics with upward magnetization (red line), downward magnetization (blue line), and no magnetization (black line). Here, the upper electrode is contacted at the middle topmost site and the upward direction is parallel to the x axis.

$\mathcal{H}_{\mathrm{P}}$ is the tight-binding Hamiltonian of the nanofiber and reads

$$\mathcal{H}_{\mathrm{P}} = \sum_{n,m} \left(\varepsilon_{nm} c_{nm}^{\dagger} c_{nm} + t_{\perp} c_{nm}^{\dagger} c_{nm+1} + t_{\parallel} c_{nm}^{\dagger} c_{n+1m} + \mathrm{H.c.} \right), \tag{2}$$

where $c_{nm}^{\dagger} = (c_{nm\uparrow}^{\dagger}, c_{nm\downarrow}^{\dagger})$ is the creation operator at site (n, m), with n the PANI index and m the site index of a PANI [Fig. 4(a)]. The number of PANIs is N, and that of aniline in a PANI is M. ε_{nm} is the on-site energy, $t_{\perp}$ the nearest-neighbor hopping integral in a PANI, and $t_{\parallel}$ the one between two successive PANIs. $\mathcal{H}_{\mathrm{SOC}}$ is the SOC Hamiltonian and reads [80,81]

$$\begin{aligned} \mathcal{H}_{\mathrm{SOC}} = \sum_{n=1}^{N-1} \sum_{m=1}^{M} & i s c_{nm}^{\dagger} \frac{r_m}{r_0} \{ [\sigma_x (\sin \varphi_{nm} + \sin \varphi_{n+1m}) \\ & - \sigma_y (\cos \varphi_{nm} + \cos \varphi_{n+1m})] \sin \theta_m \\ & + 2\sigma_z \sin \beta \cos \theta_m \} c_{n+1m} + \mathrm{H.c.} \end{aligned} \tag{3}$$

Here, s is the SOC strength, r_m the distance from site (n, m) to the helix axis (z axis), r_0 the lattice constant of a PANI, $\varphi_{nm} = (n-1)\Delta\varphi + [3 - \mathrm{sgn}(M + 1 - 2m)]\pi/2$ the azimuth angle of site (n, m), $\theta_m = \arcsin[\Delta h / l_m]$ the space angle between the vector from site (n, m) to $(n+1, m)$ and the x-y plane, $\beta = [\mathrm{sgn}(\Delta\varphi)\pi - \Delta\varphi]/2$ the deviation angle [80], and $\sigma_{x,y,z}$ the Pauli matrices. $\Delta\varphi$ and Δh

are, respectively, the twist angle and the stacking distance between two successive PANIs, $l_m = \sqrt{[(M+1-2m)r_0 \sin(\Delta\varphi/2)]^2 + (\Delta h)^2}$ the distance from site (n, m) to $(n+1, m)$, and sgn the sign function [80]. This SOC originates from electron propagation under chiral potentials [51,52]. Specifically, the SOC Hamiltonian arises only when the electrons transport between two successive PANIs because of the nanofiber chirality, whereas it vanishes for electron propagation in a single, achiral PANI. The third and fourth terms denote, respectively, the single upper nonmagnetic electrode ($\mathcal{H}_{\mathrm{U}}$) and several lower magnetic electrodes ($\mathcal{H}_{\mathrm{L}}$) and their couplings to the nanofiber, and are expressed as $\mathcal{H}_{\mathrm{U}} = \sum_k \varepsilon_{\mathrm{U}k} a^\dagger_{\mathrm{U}k} a_{\mathrm{U}k} + \tau_{\mathrm{U}} a^\dagger_{\mathrm{U}k} c_{n_{\mathrm{u}} m_{\mathrm{u}}} +$ H.c., $\mathcal{H}_{\mathrm{L}} = \sum_{j,k} \varepsilon_{\mathrm{L}_j k} a^\dagger_{\mathrm{L}_j k} a_{\mathrm{L}_j k} + \tau_{\mathrm{L}_j} a^\dagger_{\mathrm{L}_j k} c_{n_j m_j} +$ H.c. Here, τ_{U} (τ_{L_j}) is the coupling between the nanofiber and the upper nonmagnetic (jth lower magnetic) electrode. We point out that the upper electrode is connected to a single, topmost site, and the experiment can still be well fitted by numerical results when it is coupled to multiple sites of the nanofibers (see Sec. S6.1 in Supplemental Material [80]). The electrons flowing between the upper and lower electrodes are injected perpendicular to the nanofiber helix axis. Finally, the last term simulates the electron leakage from the nanofiber to the environment and is written as $\mathcal{H}_{\mathrm{d}} = \sum_{n,m,k} (\varepsilon_{nmk} d^\dagger_{nmk} d_{nmk} + t_{\mathrm{d}} d^\dagger_{nmk} c_{nm} +$ H.c.) [87].

By combining the Landauer-Büttiker formula and the Green's function method [82,83], both conductance G_{N} and current I_{N} can be obtained when the lower electrodes are magnetized upward (parallel to the x axis), so do G_{S} and I_{S} for downward magnetization [80]. In numerical calculations, the structural parameters are consistent with the experiments [78,79] and the model parameters are taken from previous works [80,84,85]. We stress that the transverse CISS effect is pronounced for extremely weak SOC of 0.6 meV and persists without any dephasing, and the experiment can be fitted in a wide range of dephasing [80].

Numerical results—Figure 4(b) shows G_{N} and G_{S} for the left-handed nanofiber contacted by the upper electrode at the middle topmost site, which are obtained at zero voltage. Although there is no SOC for electron propagation in an achiral PANI, G_{N} is different from G_{S} over almost the whole energy spectrum, indicating the emergence of transverse CISS effect. This is consistent with the experiment, demonstrating that the chirality of the nanofiber instead of the PANI monomer plays an important role in generating the transverse CISS. We point out that, for achiral nanofibers, no spin selectivity can be obtained along the helix axis or the direction normal to it, further confirming that the spin selectivity of helical nanofibers originates from their handedness. This transverse CISS, where the spin selectivity is measured along the direction normal to the helix axis, exhibits a fundamental difference from the longitudinal CISS where it is obtained along the helix axis (see Sec. S6.3 in Supplemental Material [80]). Besides, the conductances satisfy $G_{\mathrm{N}}(E) = G_{\mathrm{S}}(-E)$, owing to the electron-hole-type symmetry [88].

We then calculate the current by choosing the Fermi energy as the fitting parameter. Figure 4(c) displays the currents I_{N} and I_{S} for the left-handed nanofiber by setting the Fermi energy $E_{\mathrm{F}} = -0.9$ eV [see the vertical-dashed line of Fig. 4(b)], where the current without magnetization is shown for reference. It is clear that I_{S} is always greater than I_{N}, indicating that spin-down electrons can propagate through the left-handed nanofiber more efficiently than spin-up ones. In the absence of magnetization, the current falls between I_{S} and I_{N}. All these results are consistent with the experiment. Notice that the calculated current is one order of magnitude larger than the experimental data, because the disorder effect is ignored.

Figure 3(a) plots the numerical results of voltage-dependent SP for both nanofibers [86], where the upper electrode is contacted at the middle (second) topmost site of the left(right)-handed nanofiber [80], as sketched by the black (orange) line. We can see that the numerical results are quantitatively consistent with the experiment, especially for the right-handed nanofiber, where the voltage-dependent SP from numerical calculations almost overlaps the experimental data [see the blue circles and orange line in Fig. 3(a)]. This indicates that quantitative agreement between experiments and numerical calculations can be achieved by our theoretical model. Although the SOC is extremely weak, the SP can reach 69.6% (−73.1%) for the left(right)-handed nanofiber. This high SP arises from the combined effects of quantum interference among different transport pathways [66,89] and accumulation of weak local effect for electron propagation in such large systems. Besides, the SP exhibits mirror symmetry and decreases with the voltage V_{b} for both nanofibers, as discussed below. We take the left-handed nanofiber as an example. When the voltage approaches zero, the electron transport is determined by electronic states around the Fermi energy E_{F} and the nanofiber exhibits high SP because of large difference between G_{N} and G_{S} around E_{F} [Fig. 4(b)]. By increasing V_{b}, the electronic states within the range $[E_{\mathrm{F}} - eV_{\mathrm{b}}/2, E_{\mathrm{F}} + eV_{\mathrm{b}}/2]$ will contribute to the current. Nevertheless, the difference between G_{N} and G_{S} shrinks when the electron energy E deviates from E_{F}, and G_{N} can be greater than G_{S} for $E > 0.2$ eV [Fig. 4(b)]. Consequently, the SP of the left-handed nanofiber decreases with increasing V_{b}, so does the right-handed nanofiber.

We point out that for the transverse CISS, the SP is reversed by only flipping the nanofiber handedness [80], which is identical to the longitudinal CISS reported in various chiral molecules [21,36,37,44,51,52]. Finally, Fig. 3(b) shows the SP at $V_{\mathrm{b}} = 1$ V for both nanofibers when contacted by the upper electrode at a different topmost site (black and orange lines). One can see that the absolute value of SP of both nanofibers ranges from

55.7% to 63.4% by changing the contact position, quantitatively consistent with the experiment. Besides, the *SP* for both nanofibers is symmetric with respect to the middle topmost site due to the rotational symmetry [80]. Based on the current theoretical model, we further unveil that the nanofibers also exhibit longitudinal CISS for electrons injected parallel to the helix axis [80], consistent with previous experiment [35]. This demonstrates that our theory can interpret not only the transverse CISS but also the longitudinal CISS, thereby providing a unifying mechanism to elucidate a number of CISS experiments.

In summary, we propose a theoretical model to study the transverse CISS in chiral molecules and quantitatively explain the transverse CISS experiment. The results reveal that our theory provides a possible unifying scheme to interpret a number of CISS experiments, quantitative agreement between experiments and theory can be achieved by weak spin-orbit coupling, and the supramolecular handedness is sufficient for spin selectivity without any chiral species.

Acknowledgments—We gratefully acknowledge support from the National Natural Science Foundation of China (52273169, 12274466, 11874428, 11921005, and 12374034), the National Key Research and Development Program of China (2021YFA1200302), the Strategic Priority Research Program of the Chinese Academy of Sciences (XDB36000000), the Innovation Program for Quantum Science and Technology (2021ZD0302403), the Hunan Provincial Science Fund for Distinguished Young Scholars (2023JJ10058), and the High Performance Computing Center of Central South University.

[1] K. Ray, S. P. Ananthavel, D. H. Waldeck, and R. Naaman, Asymmetric scattering of polarized electrons by organized organic films of chiral molecules, Science **283**, 814 (1999).

[2] R. Naaman and D. H. Waldeck, Chiral-induced spin selectivity effect, J. Phys. Chem. Lett. **3**, 2178 (2012).

[3] R. Naaman and D. H. Waldeck, Spintronics and chirality: Spin selectivity in electron transport through chiral molecules, Annu. Rev. Phys. Chem. **66**, 263 (2015).

[4] R. Naaman, Y. Paltiel, and D. H. Waldeck, Chiral molecules and the electron spin, Nat. Rev. Chem. **3**, 250 (2019).

[5] O. Ben Dor, S. Yochelis, S. P. Mathew, R. Naaman, and Y. Paltiel, A chiral-based magnetic memory device without a permanent magnet, Nat. Commun. **4**, 2256 (2013).

[6] G. Koplovitz, D. Primc, O. Ben Dor, S. Yochelis, D. Rotem, D. Porath, and Y. Paltiel, Magnetic nanoplatelet-based spin memory device operating at ambient temperatures, Adv. Mater. **29**, 1606748 (2017).

[7] H. Al-Bustami, G. Koplovitz, D. Primc, S. Yochelis, E. Capua, D. Porath, R. Naaman, and Y. Paltiel, Single nanoparticle magnetic spin memristor, Small **14**, 1801249 (2018).

[8] H. Al-Bustami, B. P. Bloom, A. Ziv, S. Goldring, S. Yochelis, R. Naaman, D. H. Waldeck, and Y. Paltiel, Optical multilevel spin bit device using chiral quantum dots, Nano Lett. **20**, 8675 (2020).

[9] N. Goren, T. K. Das, N. Brown, S. Gilead, S. Yochelis, E. Gazit, R. Naaman, and Y. Paltiel, Metal organic spin transistor, Nano Lett. **21**, 8657 (2021).

[10] K. Banerjee-Ghosh, O. B. Dor, F. Tassinari, E. Capua, S. Yochelis, A. Capua, S.-H. Yang, S. S. P. Parkin, S. Sarkar, L. Kronik, L. T. Baczewski, R. Naaman, and Y. Paltiel, Separation of enantiomers by their enantiospecific interaction with achiral magnetic substrates, Science **360**, 1331 (2018).

[11] F. Tassinari, J. Steidel, S. Paltiel, C. Fontanesi, M. Lahav, Y. Paltiel, and R. Naaman, Enantioseparation by crystallization using magnetic substrates, Chem. Sci. **10**, 5246 (2019).

[12] A. Dianat, R. Gutierrez, H. Alpern, V. Mujica, A. Ziv, S. Yochelis, O. Millo, Y. Paltiel, and G. Cuniberti, Role of exchange interactions in the magnetic response and intermolecular recognition of chiral molecules, Nano Lett. **20**, 7077 (2020).

[13] K. Santra, D. Bhowmick, Q. Zhu, T. Bendikov, and R. Naaman, A method for separating chiral enantiomers by enantiospecific interaction with ferromagnetic substrates, J. Phys. Chem. C **125**, 17530 (2021).

[14] C. Wang, A.-M. Guo, Q.-F. Sun, and Y. Yan, Efficient spin-dependent charge transmission and improved enantioselective discrimination capability in self-assembled chiral coordinated monolayers, J. Phys. Chem. Lett. **12**, 10262 (2021).

[15] J. Fransson, Charge and spin dynamics and enantioselectivity in chiral molecules, J. Phys. Chem. Lett. **13**, 808 (2022).

[16] R. Naaman, Y. Paltiel, and D. H. Waldeck, Chiral induced spin selectivity and its implications for biological functions, Annu. Rev. Biophys. **51**, 99 (2022).

[17] S. F. Ozturk and D. D. Sasselov, On the origins of life's homochirality: Inducing enantiomeric excess with spin-polarized electrons, Proc. Natl. Acad. Sci. U.S.A. **119**, e2204765119 (2022).

[18] B. P. Bloom, A. R. Waldeck, and D. H. Waldeck, Homochirality and chiral-induced spin selectivity: A new spin on the origin of life, Proc. Natl. Acad. Sci. U.S.A. **119**, e2210505119 (2022).

[19] B. Göhler, V. Hamelbeck, T. Z. Markus, M. Kettner, G. F. Hanne, Z. Vager, R. Naaman, and H. Zacharias, Spin selectivity in electron transmission through self-assembled monolayers of double-stranded DNA, Science **331**, 894 (2011).

[20] Z. Xie, T. Z. Markus, S. R. Cohen, Z. Vager, R. Gutierrez, and R. Naaman, Spin specific electron conduction through DNA oligomers, Nano Lett. **11**, 4652 (2011).

[21] T. J. Zwang, S. Hürlimann, M. G. Hill, and J. K. Barton, Helix-dependent spin filtering through the DNA duplex, J. Am. Chem. Soc. **138**, 15551 (2016).

[22] J. M. Abendroth, N. Nakatsuka, M. Ye, D. Kim, E. E. Fullerton, A. M. Andrews, and P. S. Weiss, Analyzing spin selectivity in DNA-mediated charge transfer via fluorescence microscopy, ACS Nano **11**, 7516 (2017).

[23] S. Mishra, V. S. Poonia, C. Fontanesi, R. Naaman, A. M. Fleming, and C. J. Burrows, Effect of oxidative damage on charge and spin transport in DNA, J. Am. Chem. Soc. **141**, 123 (2019).

[24] T. K. Das, F. Tassinari, R. Naaman, and J. Fransson, Temperature-dependent chiral-induced spin selectivity effect: Experiments and theory, J. Phys. Chem. C **126**, 3257 (2022).

[25] D. Mishra, T. Z. Markus, R. Naaman, M. Kettner, B. Gohler, H. Zacharias, N. Friedman, M. Sheves, and C. Fontanesi, Spin-dependent electron transmission through bacteriorhodopsin embedded in purple membrane, Proc. Natl. Acad. Sci. U.S.A. **110**, 14872 (2013).

[26] M. Kettner, B. Göhler, H. Zacharias, D. Mishra, V. Kiran, R. Naaman, C. Fontanesi, D. H. Waldeck, S. Sek, J. Pawłowski, and J. Juhaniewicz, Spin filtering in electron transport through chiral oligopeptides, J. Phys. Chem. C **119**, 14542 (2015).

[27] H. Einati, D. Mishra, N. Friedman, M. Sheves, and R. Naaman, Light-controlled spin filtering in bacteriorhodopsin, Nano Lett. **15**, 1052 (2015).

[28] A. C. Aragonès, E. Medina, M. Ferrer-Huerta, N. Gimeno, M. Teixidó, J. L. Palma, N. Tao, J. M. Ugalde, E. Giralt, I. Díez-Pérez, and V. Mujica, Measuring the spin-polarization power of a single chiral molecule, Small **13**, 1602519 (2017).

[29] S. Mishra, A. K. Mondal, S. Pal, T. Kumar Das, E. Z. B. Smolinsky, G. Siligardi, and R. Naaman, Length-dependent electron spin polarization in oligopeptides and DNA, J. Phys. Chem. C **124**, 10776 (2020).

[30] T. Liu, X. Wang, H. Wang, G. Shi, F. Gao, H. Feng, H. Deng, L. Hu, E. Lochner, P. Schlottmann, S. von Molnár, Y. Li, J. Zhao, and P. Xiong, Linear and nonlinear two-terminal spin-valve effect from chirality-induced spin selectivity, ACS Nano **14**, 15983 (2020).

[31] P. C. Mondal, N. Kantor-Uriel, S. P. Mathew, F. Tassinari, C. Fontanesi, and R. Naaman, Chiral conductive polymers as spin filters, Adv. Mater. **27**, 1924 (2015).

[32] P. C. Mondal, C. Fontanesi, D. H. Waldeck, and R. Naaman, Spin-dependent transport through chiral molecules studied by spin-dependent electrochemistry, Acc. Chem. Res. **49**, 2560 (2016).

[33] S. Mishra, A. K. Mondal, E. Z. B. Smolinsky, R. Naaman, K. Maeda, T. Nishimura, T. Taniguchi, T. Yoshida, K. Takayama, and E. Yashima, Spin filtering along chiral polymers, Angew. Chem., Int. Ed. **59**, 14671 (2020).

[34] C. Kulkarni, A. K. Mondal, T. K. Das, G. Grinbom, F. Tassinari, M. F. J. Mabesoone, E. W. Meijer, and R. Naaman, Highly efficient and tunable filtering of electrons' spin by supramolecular chirality of nanofiber-based materials, Adv. Mater. **32**, 1904965 (2020).

[35] L. Jia, C. Wang, Y. Zhang, L. Yang, and Y. Yan, Efficient spin selectivity in self-assembled superhelical conducting polymer microfibers, ACS Nano **14**, 6607 (2020).

[36] V. Kiran, S. P. Mathew, S. R. Cohen, I. H. Delgado, J. Lacour, and R. Naaman, Helicenes–A new class of organic spin filter, Adv. Mater. **28**, 1957 (2016).

[37] M. Kettner, V. V. Maslyuk, D. Nürenberg, J. Seibel, R. Gutierrez, G. Cuniberti, K.-H. Ernst, and H. Zacharias, Chirality-dependent electron spin filtering by molecular monolayers of helicenes, J. Phys. Chem. Lett. **9**, 2025 (2018).

[38] M. R. Safari, F. Matthes, K.-H. Ernst, D. E. Bürgler, and C. M. Schneider, Deposition of chiral heptahelicene molecules on ferromagnetic Co and Fe thin-film substrates, Nanomaterials **12**, 3281 (2022).

[39] S. P. Mathew, P. C. Mondal, H. Moshe, Y. Mastai, and R. Naaman, Non-magnetic organic/inorganic spin injector at room temperature, Appl. Phys. Lett. **105**, 242408 (2014).

[40] P. C. Mondal, C. Fontanesi, D. H. Waldeck, and R. Naaman, Field and chirality effects on electrochemical charge transfer rates: Spin dependent electrochemistry, ACS Nano **9**, 3377 (2015).

[41] B. P. Bloom, V. Kiran, V. Varade, R. Naaman, and D. H. Waldeck, Spin selective charge transport through cysteine capped CdSe quantum dots, Nano Lett. **16**, 4583 (2016).

[42] B. P. Bloom, B. M. Graff, S. Ghosh, D. N. Beratan, and D. H. Waldeck, Chirality control of electron transfer in quantum dot assemblies, J. Am. Chem. Soc. **139**, 9038 (2017).

[43] C. Clever, E. Wierzbinski, B. P. Bloom, Y. Lu, H. M. Grimm, S. R. Rao, W. S. Horne, and D. H. Waldeck, Benchmarking chiral induced spin selectivity measurements-towards meaningful comparisons of chiral biomolecule spin polarizations, Isr. J. Chem. **62**, e202200045 (2022).

[44] M. Suda, Y. Thathong, V. Promarak, H. Kojima, M. Nakamura, T. Shiraogawa, M. Ehara, and H. M. Yamamoto, Light-driven molecular switch for reconfigurable spin filters, Nat. Commun. **10**, 2455 (2019).

[45] H. Lu, J. Wang, C. Xiao, X. Pan, X. Chen, R. Brunecky, J. J. Berry, K. Zhu, M. C. Beard, and Z. V. Vardeny, Spin-dependent charge transport through 2D chiral hybrid lead-iodide perovskites, Sci. Adv. **5**, eaay0571 (2019).

[46] Y.-H. Kim, Y. Zhai, H. Lu, X. Pan, C. Xiao, E. A. Gaulding, S. P. Harvey, J. J. Berry, Z. V. Vardeny, J. M. Luther, and M. C. Beard, Chiral-induced spin selectivity enables a room-temperature spin light-emitting diode, Science **371**, 1129 (2021).

[47] Q. Qian, H. Ren, J. Zhou, Z. Wan, J. Zhou, X. Yan, J. Cai, P. Wang, B. Li, Z. Sofer, B. Li, X. Duan, X. Pan, Y. Huang, and X. Duan, Chiral molecular intercalation superlattices, Nature (London) **606**, 902 (2022).

[48] R. Nakajima, D. Hirobe, G. Kawaguchi, Y. Nabei, T. Sato, T. Narushima, H. Okamoto, and H. M. Yamamoto, Giant spin polarization and a pair of antiparallel spins in a chiral superconductor, Nature (London) **613**, 479 (2023).

[49] P. V. Möllers, S. Ulku, D. Jayarathna, F. Tassinari, D. Nürenberg, R. Naaman, C. Achim, and H. Zacharias, Spin-selective electron transmission through self-assembled monolayers of double-stranded peptide nucleic acid, Chirality **33**, 93 (2021).

[50] C.-H. Ko, Q. Zhu, F. Tassinari, G. Bullard, P. Zhang, D. N. Beratan, R. Naaman, and M. J. Therien, Twisted molecular wires polarize spin currents at room temperature, Proc. Natl. Acad. Sci. U.S.A. **119**, e2116180119 (2022).

[51] A.-M. Guo and Q.-F. Sun, Spin-selective transport of electrons in DNA double helix, Phys. Rev. Lett. **108**, 218102 (2012).

[52] A.-M. Guo and Q.-F. Sun, Spin-dependent electron transport in protein-like single-helical molecules, Proc. Natl. Acad. Sci. U.S.A. **111**, 11658 (2014).

[53] A.-M. Guo, E. Díaz, C. Gaul, R. Gutierrez, F. Domínguez-Adame, G. Cuniberti, and Q.-F. Sun, Contact effects in spin

transport along double-helical molecules, Phys. Rev. B **89**, 205434 (2014).

[54] E. Medina, F. López, M. A. Ratner, and V. Mujica, Chiral molecular films as electron polarizers and polarization modulators, Europhys. Lett. **99**, 17006 (2012).

[55] A. A. Eremko and V. M. Loktev, Spin sensitive electron transmission through helical potentials, Phys. Rev. B **88**, 165409 (2013).

[56] S. Varela, V. Mujica, and E. Medina, Effective spin-orbit couplings in an analytical tight-binding model of DNA: Spin filtering and chiral spin transport, Phys. Rev. B **93**, 155436 (2016).

[57] S. Matityahu, Y. Utsumi, A. Aharony, O. Entin-Wohlman, and C. A. Balseiro, Spin-dependent transport through a chiral molecule in the presence of spin-orbit interaction and nonunitary effects, Phys. Rev. B **93**, 075407 (2016).

[58] V. V. Maslyuk, R. Gutierrez, A. Dianat, V. Mujica, and G. Cuniberti, Enhanced magnetoresistance in chiral molecular junctions, J. Phys. Chem. Lett. **9**, 5453 (2018).

[59] K. Michaeli and R. Naaman, Origin of spin-dependent tunneling through chiral molecules, J. Phys. Chem. C **123**, 17043 (2019).

[60] S. Dalum and P. Hedegård, Theory of chiral induced spin selectivity, Nano Lett. **19**, 5253 (2019).

[61] M. Geyer, R. Gutierrez, V. Mujica, and G. Cuniberti, Chirality-induced spin selectivity in a coarse-grained tight-binding model for helicene, J. Phys. Chem. C **123**, 27230 (2019).

[62] G.-F. Du, H.-H. Fu, and R. Wu, Vibration-enhanced spin-selective transport of electrons in the DNA double helix, Phys. Rev. B **102**, 035431 (2020).

[63] Y. Utsumi, O. Entin-Wohlman, and A. Aharony, Spin selectivity through time-reversal symmetric helical junctions, Phys. Rev. B **102**, 035445 (2020).

[64] L. Zhang, Y. Hao, W. Qin, S. Xie, and F. Qu, Chiral-induced spin selectivity: A polaron transport model, Phys. Rev. B **102**, 214303 (2020).

[65] X. Yang, C. H. van der Wal, and B. J. van Wees, Detecting chirality in two-terminal electronic nanodevices, Nano Lett. **20**, 6148 (2020).

[66] P.-J. Hu, S.-X. Wang, X.-H. Gao, Y.-Y. Zhang, T.-F. Fang, A.-M. Guo, and Q.-F. Sun, Spin-dependent electron transport along hairpinlike DNA molecules, Phys. Rev. B **102**, 195406 (2020).

[67] J. Fransson, Vibrational origin of exchange splitting and chiral-induced spin selectivity, Phys. Rev. B **102**, 235416 (2020).

[68] S. Alwan and Y. Dubi, Spinterface origin for the chirality-induced spin-selectivity effect, J. Am. Chem. Soc. **143**, 14235 (2021).

[69] Y. Liu, J. Xiao, J. Koo, and B. Yan, Chirality-driven topological electronic structure of DNA-like materials, Nat. Mater. **20**, 638 (2021).

[70] Y. Wolf, Y. Liu, J. Xiao, N. Park, and B. Yan, Unusual spin polarization in the chirality-induced spin selectivity, ACS Nano **16**, 18601 (2022).

[71] S. Varela, M. Peralta, V. Mujica, B. Berche, and E. Medina, Spin polarization induced by decoherence in a tunneling one-dimensional Rashba model, SciPost Phys. Core **6**, 044 (2023).

[72] A. K. Mondal, M. D. Preuss, M. L. Śleczkowski, T. K. Das, G. Vantomme, E. W. Meijer, and R. Naaman, Spin filtering in supramolecular polymers assembled from achiral monomers mediated by chiral solvents, J. Am. Chem. Soc. **143**, 7189 (2021).

[73] Y. Sang, Q. Zhu, X. Zhou, Y. Jiang, L. Zhang, and M. Liu, Ultrasound-directed symmetry breaking and spin filtering of supramolecular assemblies from only achiral building blocks, Angew. Chem., Int. Ed. **62**, e202215867 (2023).

[74] D. H. Waldeck, R. Naaman, and Y. Paltiel, The spin selectivity effect in chiral materials, APL Mater. **9**, 040902 (2021).

[75] F. Evers *et al.*, Theory of chirality induced spin selectivity: Progress and challenges, Adv. Mater. **34**, 2106629 (2022).

[76] C. D. Aiello *et al.*, A chirality-based quantum leap, ACS Nano **16**, 4989 (2022).

[77] B. P. Bloom, Y. Paltiel, R. Naaman, and D. H. Waldeck, Chiral induced spin selectivity, Chem. Rev. **124**, 1950 (2024).

[78] C. Zhou, Y. Ren, J. Han, X. Gong, Z. Wei, J. Xie, and R. Guo, Controllable supramolecular chiral twisted nanoribbons from achiral conjugated oligoaniline derivatives, J. Am. Chem. Soc. **140**, 9417 (2018).

[79] C. Zhou, Y. Ren, J. Han, Q. Xu, and R. Guo, Chiral polyaniline hollow nanotwists toward efficient enantioselective separation of amino acids, ACS Nano **13**, 3534 (2019).

[80] See Supplemental Material at http://link.aps.org/supplemental/10.1103/PhysRevLett.133.108001 for (i) experimental procedures, (ii) theoretical methods, (iii) additional experimental data, (iv) structural parameters, (v) SOC Hamiltonian and model parameters, and (6) additional numerical results, which includes Refs. [21,32,35,78,79,81–85].

[81] D. Hochberg, G. Edwards, and T. W. Kephart, Representing structural information of helical charge distributions in cylindrical coordinates, Phys. Rev. E **55**, 3765 (1997).

[82] S. Datta, *Electronic Transport in Mesoscopic Systems* (Cambridge University Press, Cambridge, England, 1997).

[83] N.-X. Yang, Y.-F. Zhou, Z. Hou, and Q.-F. Sun, Anomalous spin Nernst effect in Weyl semimetals, J. Phys. Condens. Matter **31**, 435301 (2019).

[84] F. Tournus, S. Latil, M. I. Heggie, and J.-C. Charlier, π-stacking interaction between carbon nanotubes and organic molecules, Phys. Rev. B **72**, 075431 (2005).

[85] S. Che, P. Stepanov, S. Ge, M. Zhu, D. Wang, Y. Lee, K. Myhro, Y. Shi, R. Chen, Z. Pi, C. Pan, B. Cheng, T. Taniguchi, K. Watanabe, Y. Barlas, R. K. Lake, M. Bockrath, J. Hwang, and C. N. Lau, Substrate-dependent band structures in trilayer graphene/h-BN heterostructures, Phys. Rev. Lett. **125**, 246401 (2020).

[86] Since I_S and I_N, measured in the experiment, contain both spin-up and spin-down components, this definition of *SP* refers to magnetoconductance, see T. Liu and P. S. Weiss, Spin polarization in transport studies of chirality-induced spin selectivity, ACS Nano **17**, 19502 (2023). In numerical

calculations, I_S and I_N also contain spin-up and spin-down components, which are the same as the experiment.

[87] The dephasing can arise from the electron-phonon interaction, the electron-electron interaction, and the contact with a thermal reservoir, which has been widely studied in previous works regarding the longitudinal CISS, see Refs. [24,51,52,57,62,71].

[88] A.-M. Guo, T.-R. Pan, T.-F. Fang, X. C. Xie, and Q.-F. Sun, Spin selectivity effect in achiral molecular systems, Phys. Rev. B **94**, 165409 (2016).

[89] T.-R. Pan, A.-M. Guo, and Q.-F. Sun, Spin-polarized electron transport through helicene molecular junctions, Phys. Rev. B **94**, 235448 (2016).